

THE ORIGIN OF THE ASSYMETRY IN THE ICELAND HOTSPOT ALONG  
THE MID-ATLANTIC RIDGE FROM CONTINENTAL BREAKUP TO  
PRESENT-DAY

A THESIS SUBMITTED TO THE GRADUATE DIVISION OF THE  
UNIVERSITY OF HAWAI'I AT MĀNOA IN PARTIAL FULFILLMENT OF  
THE REQUIREMENTS FOR THE DEGREE OF

MASTER OF SCIENCE

IN

GEOLOGY AND GEOPHYSICS

AUGUST 2013

By

Samuel M. Howell

Thesis Committee:

Garrett Ito, Chairperson  
John Sinton  
Clint Conrad

## **Abstract**

The Iceland hotspot has interacted asymmetrically with the Mid-Atlantic ridge since continental breakup, influencing the Reykjanes Ridge over a greater distance to the south than the Aegir and Kolbeinsey Ridges to the north. We investigate causes of this asymmetry with 3D numerical models that simulate a mantle plume interacting with the evolving ridge system. Modeled maps of crustal thickness and plume influence indicate that asymmetrical influence along the ridge system is partially caused by the asymmetric ridge configuration relative to the hotspot center, and is either enhanced by variations thermal lithosphere thickness or largely unchanged when the lithosphere is created by extraction of water at the base of the melting zone. Comparisons of model predictions with geophysical estimates of asymmetry and crustal thickness variations along the ridges suggest the Iceland plume volume flux is 100-200 m<sup>3</sup>/s and the dehydration stiffens the upper mantle, but to a lesser degree than simulated.

## Table of Contents

i	Abstract .....	i
ii	List of Tables .....	iii
iii	List of Figures .....	iv
1	Introduction .....	1
2	Methods .....	3
2.1	Model Setup .....	3
2.2	Mantle melting and crustal accretion .....	4
2.3	Tracking plume material .....	4
2.4	Model parameters .....	5
3	Model Results .....	7
3.1	General temporal behavior of the plume .....	7
3.2	Record of plume influence on the seafloor .....	7
3.3	Dependence of plume asymmetry on plume volume flux, viscosity, and rheology .....	9
4	Discussion: Comparison of Model Predictions with Observations .....	10
4.1	Asymmetry and plume influence .....	10
4.2	Crustal thickness .....	11
5	Conclusions .....	13
6	References .....	25

**List of Tables**

1 Varied model parameters ..... 6

## List of Figures

1	Residual basement topography of the North Atlantic .....	14
2	Plate reconstructions and paleo-basement depth from 55-10 Ma .....	15
3	Mean North Atlantic spreading rate history from 55-0 Ma .....	16
4	Example model output and lithosphere type illustration .....	17
5	Example plume “pancake” evolution from 54-0 Ma .....	18
6	Model output maps of crustal thickness and plume influence.....	19
7	Modeled radial and width symmetry versus plume flux .....	20
8	Crustal thickness profile comparisons between models and observations at the Aegir Ridge .....	21
9	Crustal thickness profile and comparisons between models and observations along the Reykjanes and Kolbeinsey Ridges .....	22

## CHAPTER 1. INTRODUCTION

The North Atlantic Ocean Basin has been heavily influenced by excess volcanism associated with the Iceland Hotspot from prior to the time of continental break-up until present-day. For example, residual basement topography (bathymetry corrected for sedimentation and subsidence with seafloor age) is anomalously shallow for  $>2,000$  km along the margins of Greenland and Norway, and becomes increasingly shallow in the basin towards Iceland (Figure 1). This shallow seafloor region comprises the North Atlantic Igneous Province (e.g. Coffin and Eldholm, 1994; Holbrook et al., 2001; White, 1997). Northeast of Iceland, shallow topography surrounds the basin created by the now-extinct Aegir Ridge (AR), however, most of the AR basin is not anomalously shallow. Apparently, the hotspot heavily influenced the areas west, east, and south of the basin, but for some reason did not influence much of the AR basin itself. Another peculiar aspect of Iceland hotspot influence is that it appears to extend less far north along the Kolbeinsey Ridge (KR) compared to south along the Reykjanes Ridge (RR) relative to Vatnajökull volcano (e.g. Hooft et al., 2006; Schilling, 1999; Schilling et al., 1983), which marks the center of the Iceland hotspot as confirmed by upper mantle tomography (Allen et al., 2002; Wolfe et al., 1997). Thus, the Iceland hotspot appears to have asymmetrically influenced North Atlantic spreading and crustal production throughout much of its history.

The tectonic evolution of the area might reveal clues to potential causes of North Atlantic asymmetry. The breakup of Greenland and Norway initiated  $\sim 55$  Ma and ensued with extensive flood basalt volcanism along the continental margins to form a major magmatic phase of the igneous province. Seismic studies document igneous crustal thicknesses of up to  $\sim 35$  km along both continental margins near the center of the Iceland hotspot track, and thicknesses  $\geq 15$  km extending  $\geq 1,000$  km along the margins to the north and south (Breivik et al., 2006; Holbrook et al., 2001; Mjelde et al., 2008; Voss et al., 2009). Shortly after breakup, oceanic crust began forming along three main ridge segments, the RR, AR, and Mohns Ridge (MR) (Figure 2). For the first couple million years after continental breakup ( $\sim 55$ -53 Ma), average half-spreading rates (29-33 km/Myr) and crustal thickness were maximal (Figure 3). For example, oceanic crustal thickness was  $\sim 8$  km at the AR (Breivik et al., 2006) (Figure 3) and was as thick or thicker along much of the RR, and certainly the Iceland-Greenland and Iceland-Faeroe ridges (e.g. Holbrook et al., 2001; Smallwood et al., 1999). At this time, the relative location of the hotspot center was likely near the margin of east Greenland (Figure 2), although the lack of a documented age progression along the presumed hotspot track leads to large uncertainties in the relative location of the hotspot through time (e.g. Lawver and Müller, 1994; Mihalfy et al., 2008; Steinberger, 2000). In pre- and early-rift history, hotspot influence was widespread and no clear asymmetry is noted.

During  $\sim 52$ -43 Ma, the average seafloor half-spreading rate along the three ridges slowed to  $\sim 12$  cm/yr, and the influence of the hotspot on the AR decreased significantly (Figure 3). During 43-28 Ma, evidence shows that the spreading rate along the AR probably deviated from that along the RR and MR, with the AR spreading  $<70\%$  as fast (Breivik et al., 2006; Mosar et al.,

2002; Smallwood and White, 2002; Voss et al., 2009), perhaps related to lithospheric stretching or the very earliest stages of rifting at the KR. The crust generated was only 3.5-5.5 km in thickness at the middle and northern portions of the AR (Breivik et al., 2006; Rai et al., 2012), clearly not elevated compared to normal (not hotspot influenced) oceanic crust at the same slow spreading rate (Dick et al., 2003; White et al., 2001). Somewhat thickened crust (8 km) is apparent only to the south of the AR at ~29 Ma (Rai et al., 2012).

By 28 Ma, seafloor spreading had begun migrating from south to north along the KR, separating the Jan Mayen Microcontinent (JMMC) from East Greenland (Figure 2). At ~25 Ma, the AR ceased spreading, and the KR accommodated all spreading in this compartment of the North Atlantic. Plume influence along the RR at this time is inferred from smooth seafloor created by the part of the RR spreading obliquely in the north without any prominent transform faults, in contrast to the rougher seafloor to the south created by orthogonal spreading along segments separated by transform faults (White, 1997). The extent of plume influence along the RR as seen in the “rough-smooth boundary” extended some 600-1200 km southwest of the Iceland hotspot along the RR. However, this distance projected northeast would encompass a large portion, if not all, of the AR. The lack of thickened crust along most of the AR during all but the first 2-3 Myr of its spreading history suggests that the plume influence was asymmetric starting near 47 Ma, influencing the RR further southwest than the AR to the northeast.

When considering the tectonic evolution of this system, some hypotheses can be formulated as to the cause of this apparent asymmetry in hotspot influence. (1) The rifting of the Jan Mayen Microcontinent (JMMC) and the resultant lithospheric protrusion inhibited plume material from reaching the AR. (2) The closer proximity of the RR to the hotspot center, and offset between the AR and the hotspot center preferentially promoted dissemination of plume material south along the RR. (3) Westward North American plate motion inhibited eastward flow of plume material to AR.

To test the above hypotheses about the AR basin and address the broader problem of asymmetric Iceland hotspot influence, we use 3-D numerical models that simulate a plume interacting with rifting continents and spreading ridges. The models simulate mostly-realistic ridge geometries and historical spreading rates since the time of continental break-up (~55 Ma) to present-day. Variables of the model include plume volume flux, mantle viscosity, and the structure of the lithosphere. In one set of models, temperature alone controls lithospheric structure, resulting in lithosphere that is thinnest beneath the ridge axes and thickest beneath the continents; in another set, the structure is controlled by water content, where partial melting removes water from the solid and leaves a stiff, compositional lithosphere. We quantify the effects of the above parameters and constrain the mantle dynamic processes that likely influence the asymmetry of the hotspot influence and create the apparent “hole” in influence at the Aegir Basin.

## CHAPTER 2. METHODS

### 2.1 Model setup

We employ Citcom, a finite element code widely used to simulate mantle convection (e.g. Moresi and Gurnis, 1996; Zhong et al., 2000). Citcom solves the equations describing conservation of mass, conservation of momentum, and conservation of energy in a Cartesian coordinate system for a fluid with zero-Reynolds number and infinite Prandtl number. The extended Boussinesq approximation simulates the adiabatic temperature gradient and latent heat loss due to melting (Bianco et al. 2011). Model dimensions are  $2400 \times 2800 \times 400$  km, with  $289 \times 257 \times 65$  elements in the  $x$ ,  $y$ , and  $z$  directions, respectively (Figure 4).

Modeled viscosity decreases as an Arrhenius function of temperature and increases exponentially with depth (Ballmer et al., 2007). In some models, viscosity also depends inversely on the amount of water dissolved in the solid (Hirth and Kohlstaedt, 2003). Thickness variations of the lithosphere are controlled by considering two different rheological laws. With the first, a “thermal lithosphere” results from viscosity that only depends on pressure and temperature. The thermal lithosphere corresponds to the cool thermal boundary layer near the surface (Figure 4b) and is therefore directly coupled to the geometry of the plates: it is thinnest beneath the ridges, thicker away from the ridge and beneath ridge offsets, and thickest beneath continents and the Jan Mayen micro-continent. With the second rheology, a “dehydrated lithosphere” results from the inverse dependence of viscosity on water content, whereby the extraction of water at the base of the melting zone leads to a rapid increase in viscosity by two orders of magnitude (Hirth and Kohlstedt 1996). In this case, the base of the lithosphere is thickest near the plume where the solidus is deepest and thins away from the plume center (Fig. 4c, Ito et al. 1999), but the thickness variations are small compared to those of thermal lithosphere and do not relate directly to the shape of the plates.

The plume source is imposed as a hot circular patch on the bottom boundary of the model, with a peak excess temperature of  $\Delta T = 150$  K at the plume center, decaying as a Gaussian function of radial distance, characterized by radius  $r$ , at which the temperature anomaly has decreased by a factor of  $e$ . The models simulate a plume centered on the Mid-Atlantic Ridge at all times. This is a simplification, but one that is consistent with the Greenland–Iceland and Faeroe–Iceland volcanic ridges, representing the hotspot tracks on both plates, with the hotspot being very near or at the Mid-Atlantic Ridge since continental breakup (Vink, 1984; White, 1988; White, 1997; Wilson, 1973).

Plate geometry is imposed with horizontal velocity boundary conditions on the top model surface; diverging velocities define ridge axes (Figure 4a, plate motion is in the  $x$  direction). The geometry is obtained from a polar projection of the North Atlantic reconstructed at 54 Ma (Müller et al., 2008), rotated into the average spreading direction of the region. The RR, AR, and MR are approximated with straight segments, with transforms parallel to the spreading

direction. The straight segment that approximates the RR extends through Iceland, so eastward offset of the Eastern Volcanic Zone is neglected for simplicity. An average North Atlantic spreading rate is used for all ridges, except at the AR when spreading rates significantly diverge from the average during ~43-33 Ma, and at the KR, which spreads slower than average before the death of the AR (Figure 3).

The initial conditions simulate the pre-rifted, continental lithosphere as a ~100-km-thick, cool thermal boundary layer. The surface is held motionless to allow the plume to rise from the base to the top of the model, and for it to begin spreading like a “pancake” beneath the lithosphere. Once the pancake expands to a diameter of ~2400 km—the approximate extent of influence along the Greenland continental margin (Holbrook et al., 2001)—continental rifting and the seafloor spreading sequence initiates.

## ***2.2 Mantle melting and crustal accretion***

To investigate how the evolving mantle plume affects igneous crustal thickness, we solve for melt production and compute crustal thickness. Melting rate is found by calculating the time rate of change of extent of melt depletion,  $F$ , based on the parameterization of Katz et al. (2003), and advecting  $F$  with passive tracers (Bianco et al., 2008). The melt produced is assumed to instantaneously migrate in the spreading direction to the nearest spreading segment. Crustal thickness,  $T_c$ , is computed at each point in the accretion zone (30 km wide)—centered on the ridge axis—by solving the time-dependent advection equation in the Lagrangian reference of each spreading plates, using explicit forward differencing in time,

$$\frac{DT_c}{Dt} = q_c . \quad (1)$$

The left hand side is the material time derivative of  $T_c$  and  $q_c$  is the volume flux of melt delivered from the mantle per unit area at the surface.

## ***2.3 Tracking plume material***

Passive particles are also used to track plume material. Plume markers are introduced at a depth of 200 km wherever the mantle temperature is elevated above the ambient value by  $>\Delta T/e$ . The width of plume influence is considered to be the distance along the ridge axes at which the marked plume material contributes  $>50\%$  to the model crust by volume. The widths along the Reykjanes and Aegir Ridges ( $W_{RR}$  and  $W_{AR}$ , respectively) are measured at ~30 Ma, which is near the time the AR became extinct and close to the isochron along which Rai et al. (2012) seismic refraction profile ran. In addition, the total radial distances of plume influence at 30 Ma,  $R_{RR}$  and  $R_{AR}$ , are the distance from the plume center to the most distal extent of plume influence along the RR and AR, respectively. The ratios  $W_{AR}/W_{RR}$  and  $R_{AR}/R_{RR}$  measure the asymmetry of plume influence along the AR compared to the RR. Ratios of unity represent perfect symmetry; lower values represent greater asymmetry.

## 2.4 Model parameters

Several properties are likely to influence the manner in which plume material expands. Volume plume flux,  $Q$ , is known to be one primary control on the total width,  $W$ , to which a plume expands along a ridge axis at steady-state, given the spreading rate  $U$ ;  $W \propto (Q/U)^{1/2}$  (Ribe et al., 1995). Volume flux may also modulate the asymmetry of the plume by influencing the rate of plume-buoyancy-driven mantle flow, which alone should be radially symmetric, relative to plate-driven mantle flow, which in the North Atlantic is asymmetric. Finally, by varying  $Q$  and viscosity,  $\eta$ , we vary the characteristic thickness of the plume material ponding beneath the lithosphere,  $S_0$  (Ribe et al., 1995).

$$S_0 = \left( \frac{48\eta Q}{g\Delta\rho} \right)^{1/4}. \quad (2)$$

Here,  $g$  is gravitational acceleration, and  $\Delta\rho$  is the density contrast between the plume and the ambient mantle. The ratio of  $S$  relative to the thickness variations of the lithosphere is predicted to control the degree to which lithosphere structure influences the lateral expansion of the plume pancake (Ribe et al. 1996). If the ratio is large, then the pancake expands much like it would against a flat surface, whereas if the ratio is close to one, the expansion can be perturbed by a sloping base of the lithosphere (Ribe et al. 1996). When calculating  $S$ , the lowest viscosity in the ponding plume pancake is assigned to  $\eta$ . In models of a dehydrated lithosphere,  $S$  pertains to the characteristic thickness of the hot layer below the dehydrated layer. If the lithosphere is thermally controlled, then the pattern of lithosphere thickness variations relates directly to asymmetric geometry of the ridges with respect to the plume center. Thus, models of a thermal lithosphere should tend to lead to larger asymmetries than those of a dehydrated lithosphere.

To modulate  $Q$ ,  $\eta$ , and the ratio of  $S$  to thickness variations of the lithosphere, we vary three model input parameters: plume radius,  $r$ , Rayleigh number,  $Ra$  (higher  $Ra$  simulates lower plume viscosities), and water-independent versus water-dependent rheology (details given in Table 1). Reference mantle potential temperature (1325°C – 1338°C) varies with Rayleigh number to produce reasonable (5.5-6.5 km) crustal thicknesses for non-plume influenced, slow-spreading ridges (Dick et al., 2003; White et al., 2001). A range of plume volume fluxes are investigated (95 - 450 m<sup>3</sup>/s) by varying plume radius (65 - 180 km) at two Rayleigh numbers ( $5 \times 10^5$  and  $2 \times 10^6$ ). About half of the calculations simulate a thermal lithosphere without the effects of dehydration stiffening, and about half consider a dehydrated lithosphere that includes these effects. Model outputs are maps of crustal thickness, volume fraction of plume-contributed crust and model seafloor ages, along with the widths ( $W_{RR}$  and  $W_{AR}$ ) and radial distances ( $R_{RR}$  and  $R_{AR}$ ) of plume influence along the Aegir and Reykjanes Ridges.

**Table 1:** Model parameters varied (all other parameters were kept constant).

Parameter	$Ra$	$T_p$	$r$	$Q$	
Definition	Rayleigh number	Mantle Potential Temperature	Plume Radius	Plume Volume Flux	Rheology
Units	Dimensionless	$^{\circ}C$	km	$m^3/s$	
Model 1a	$0.5 \times 10^6$	1338	0	0	no dehydration
Model 1b	$0.5 \times 10^6$	1338	0	0	dehydration
Model 2a	$0.5 \times 10^6$	1338	95	114	no dehydration
Model 2b	$0.5 \times 10^6$	1338	95	95	dehydration
Model 3a	$0.5 \times 10^6$	1338	130	232	no dehydration
Model 3b	$0.5 \times 10^6$	1338	130	178	dehydration
Model 4	$0.5 \times 10^6$	1338	149	226	dehydration
Model 5a	$0.5 \times 10^6$	1338	180	446	no dehydration
Model 5b	$0.5 \times 10^6$	1338	180	303	dehydration
Model 6a	$1.0 \times 10^6$	1332	105	272	no dehydration
Model 6b	$1.0 \times 10^6$	1332	120	275	dehydration
Model 7a	$1.5 \times 10^6$	1328	89	263	no dehydration
Model 7b	$1.5 \times 10^6$	1328	102	289	dehydration
Model 8a	$2.0 \times 10^6$	1325	65	146	no dehydration
Model 8b	$2.0 \times 10^6$	1325	65	128	dehydration
Model 9a	$2.0 \times 10^6$	1325	82	276	no dehydration
Model 9b	$2.0 \times 10^6$	1325	88	268	dehydration
Model 10a	$2.0 \times 10^6$	1325	130	840	no dehydration
Model 10b	$2.0 \times 10^6$	1325	130	597	dehydration

## CHAPTER 3. MODEL RESULTS

### *3.1 General temporal behavior of the plume*

The evolution of the plume in an exemplary model (Model 3a, Table 1) is shown in Figure 5. Again, the plume is first allowed to expand beneath a stationary, thick continental plate; once it spans a diameter of 2400 km, continental rifting begins. Right after continental breakup (54 Ma), the initially wide plume pancake quickly contracts as it fills the inverted trough created by the thinning lithosphere along the Mid-Atlantic Ridge. The thick continental lithosphere draws plume material away from the rift faster than it is replenished from below by the plume stem. In this case at ~47 Ma, the pancake is nearly half its original radius, but has contracted less to the SW than to the NE. The pancake is already asymmetric: it spans further along the RR than along the AR, and also is no longer present beneath the MR (Figure 5).

Just after the model time of ~47 Ma, the plume pancake begins to widen along the ridges (Figure 5) largely due to a factor of ~3 reduction in spreading rate (Figure 3). By 30 Ma, the pancake in this model is more than twice as wide along the RR as it is along the AR. The slow widening along the ridges continues in this model to ~27 Ma (not shown).

From 28-25 Ma, the rifting at the KR begins in the south and propagates north—at the expense of the AR. At 25 Ma (not shown), the AR is fully extinct, but the model shows that until ~23 Ma a small amount of melting continues beneath the AR as plume material still rises beneath the locally thin (but no longer spreading) lithosphere (Figure 5). The width of the plume pancake along the AR increases slightly and the expansion along the RR stagnates as plume material that would otherwise feed the RR now flows toward the KR. From 25-15 Ma, the plume contracts along the KR in response to continental rifting, much like the initial plume contraction event at 54 Ma. Starting ~10 Ma, the plume widens slightly along the KR. By the model time representing present-day, the plume pancake is still widening, along the KR, but has reached a minimum in width along the RR. As influence to KR increases, the still-evolving plume will approach a state of symmetrical ridge influence.

### *3.2 Record of plume influence on the seafloor*

The evolution of the system is recorded in model maps of crustal thickness and fractional contribution of the plume to the crust. Figure 6 shows maps produced by example models of two different plume fluxes, for both rheologies. The model of high plume flux and thermal lithosphere is the same model presented in Figure 5 (Model 3a, Figure 6a-d). In this (as in all) models, the plume influence initially extends maximally (2400 km) along the model continental margins. The initial contraction of the pancake immediately following continental breakup results in long (tapered) bands of plume-influenced crust along the continental margins adjacent to uninfluenced crust (Figure 6a). From the minimum in width of plume influence (after the initial contraction, near seafloor age of ~49 Ma) widths increase toward the 25 Ma isochron along both ridges, although more extensively southward along the model RR than north along

the AR. A slight retraction in influence in the model KR basin is seen as narrow bands of influenced crust along the margins at the northern end of the basin next to small patches of uninfluenced seafloor. After this retraction, plume influence widens toward the present-day KR and recedes along the RR.

Modeling a lower plume flux (Model 8a, Figure 6b), the width of influence on the seafloor is overall less than in the high flux case (Model 3a) after the initial contraction. Between the 47 and 25 Ma isochrons, plume influence is seen to widen along RR while receding slightly (rather than widening as in Model 3a) along AR. The KR basin shows streaks of wide plume influence near the rifted margins, which are less pronounced than the solid bands of influence in Model 3a. Plume influence widens toward the present-day KR from the minimum width near the continental margin. In the RR basin, the width of influence decreases between the 25 Ma isochron and the present-day RR.

In both of the models shown of a thermal lithosphere, crustal thickness (Figures 6c,d) is slightly enhanced near the continental margins (7-9 km) and greatest (90-140 km) along the volcanic ridge east and west of the plume center. However, the predicted crustal thickness at the continental margins is not overly thick, primarily because there is an artificial time lag in the model between when rifting is first imposed and when the lithosphere is thin enough to allow for substantial decompression melting. This results in suppressed melt production prior to 50 Ma. This effect was shown to be overcome in previous numerical models by initiating the lithosphere to be (~50%) thinner beneath rift zones as elsewhere in order to simulate rifting prior to the main continental breakup event (Nielsen and Hopper, 2004). On younger seafloor, small-amplitude (2-5 km), shorter-wavelength variations in crustal thickness are evident and extend 2-3 times further along RR in the high flux, compared to the low-flux case. Crust at the southern AR and KR is thickened by plume influence (11-14 km). Plume-thickened crust is present for about half the length of AR in the high-flux case (Model 3a), but is restricted to the southern quarter of the ridge in the low-flux case (Model 8a).

Relative to the above models of a thermal lithosphere, models of comparable plume fluxes with a dehydrated lithosphere predict a more dramatic initial contraction in plume influence, resulting in longer sections of plume-influenced margins adjacent to uninfluenced seafloor (Figure 6e,f). Between the conjugate 47-Ma isochrons, the overall width of plume influence is less with dehydrated lithosphere than with thermal lithosphere, with the largest difference occurring at the RR. The widths at the RR are more comparable to those at the AR indicating that the relatively flat base of the dehydrated lithosphere leads to a more symmetric plume pancake.

Models of dehydrated lithosphere produce crustal thicknesses (Figure 6g,h) slightly thinner at the margins (< 8 km) and along the east-west trending volcanic ridges (17-21 km), and lack the short-wavelength variations in crustal thickness seen in the thermal lithosphere cases. Thickened

crust extends a similar distance along the AR and KR between the two rheologies, but the models of a dehydrated lithosphere yield a smaller peak crustal thickness ( $< 9$  km) at the AR.

### **3.3 Dependence of plume asymmetry on plume volume flux, viscosity, and rheology**

Results of the radial distance ratio,  $R_{AR}/R_{RR}$ , versus plume flux for the two Rayleigh numbers,  $0.5 \times 10^6$  and  $2.0 \times 10^6$ , with and without dehydration rheologies are shown in Figure 7a. Plume flux,  $Q$ , and Rayleigh number, which is inversely proportional to plume viscosity, have no consistent influence on  $R_{AR}/R_{RR}$ . Thus, characteristic thickness,  $S$ , of the pancake (Eq. 2)—which we vary with  $Q$  and/or  $\eta$ —does not seem to influence the observed asymmetry over the range of thicknesses tested (80-180 km). The biggest difference occurs between cases with and without dehydration. With a dehydrated lithosphere, the width of influence along the AR is 70-80% that of the RR ( $R_{AR}/R_{RR}$  is  $\sim 0.7-0.8$ ). Thus, even when the lithosphere is relatively flat, models show asymmetry in plume influence to the ridge system. This result is likely due to westward shear from the North American Plate inhibiting NE plume flow to the AR, with no such inhibition SSW along the RR. This result demonstrates an inherent asymmetry in plume influence based solely on the regional ridge geometry, proving hypothesis (1) correct. With a thermal lithosphere,  $R_{AR}/R_{RR}$  is  $\sim 0.4-0.5$ , indicating even greater asymmetry. In these cases, plume influence to the AR is inhibited not only by plate shear, but also by the large difference in lithospheric thickness across the transform between the RR and AR and the relatively thick thermal lithosphere of the JMMC, which has long been predicted to inhibit mantle flow between ridges (e.g. Vogt and Johnson, 1975). These results prove hypothesis (2) also generally correct.

The ratio of widths along the AR versus the RR,  $W_{AR}/W_{RR}$  are found to increase with plume volume flux,  $Q$  (Figure 7b). The increase in  $W_{AR}/W_{RR}$  with  $Q$ —in contrast to  $R_{AR}/R_{RR}$  not changing with  $Q$ —reflects the gap between the plume center and the southern boundary of the Aegir Ridge. In a hypothetical case in which  $Q$  is low enough that  $R_{AR}$  is equal to the gap,  $W_{AR}$  and  $W_{AR}/W_{RR}$  would be zero. The proportional increase in  $W_{AR}$  with  $Q$  from this theoretical minimum is more rapidly than the proportional increase in  $W_{RR}$ .  $W_{AR}/W_{RR}$  increases more subtly with  $Q$  in models of a thermal lithosphere than in models of a dehydrated lithosphere, reflecting a tendency of the former to result in a more asymmetric plume pancake. Rayleigh number (or viscosity) still has little, or no, effect on the asymmetry as measured by  $W_{AR}/W_{RR}$ .

## CHAPTER 4. DISCUSSION: COMPARISON OF MODEL PREDICTIONS WITH OBSERVATIONS

### 4.1 Asymmetry and plume influence

Several features present in the observed residual bathymetry and the inferred extents of plume influence in the North Atlantic (Figure 1) can now be interpreted based on model predictions of plume-contributed crust. The residual bathymetry shows shallow continental margins, composed of thick igneous crust, which transitions to deeper seafloor over short seaward distances of ~100 km. This transition is predicted to occur due to the rapid reduction in width of plume influence along rifting continental margins (Figure 6). The narrowing of plume influence in the models does not require a reduction in plume flux, but results from rapid contraction of the originally (2400 km) wide plume pancake during continental rifting. An observed minimum width of plume influence is evident seaward of the initially influenced margins in contours of residual bathymetry and, in the RR basin, by the appearance of rough seafloor created by orthogonal spreading of a segmented RR (White, 1997). From this minimum width, the influence of the plume appears to have propagated farther south along the RR, which is seen as the rough-smooth boundary angling toward the present-day RR (Figure 1). This is another behavior predicted by the models (Figure 6).

Near 25 Ma, which corresponds to the time that the AR becomes extinct and KR is fully active, the rough-smooth boundary continues to slant southward toward the RR. However, models predict the plume influence to retract back north along the RR as more plume material is drawn toward the KR. The observed continued southward propagation of the rough-smooth boundary could signal an increase in the flux of the Iceland plume not simulated in the current models, possibly due to an increase in plume radius, temperature, or both. This suggests that our models best represent the period when the AR was spreading (~55-25 Ma). In the basin formed by the KR, shallow residual topography is evident along the margins of Greenland and the JMMC (Figure 1), much like the bands of plume-derived crust predicted in the models (Figure 6).

To address the actual asymmetry of the Iceland hotspot along the Mid-Atlantic Ridge, we estimate  $R_{AR}/R_{RR}$  and  $W_{AR}/W_{RR}$  using the same criteria as the model analysis, applied to the reconstructed geometry (Müller et al., 2008) of the RR and AR at 30 Ma. Distances of plume influence along the RR are found using the rough-smooth boundary in seafloor fabric, and along the AR are based on the extent of elevated crustal thickness presented in the seismic refraction profile of Rai et al. (2012). Uncertainties in the widths ( $W_{AR}$ ,  $W_{RR}$ ) and radial distances ( $R_{AR}$ ,  $R_{RR}$ ) include the uncertainty in the location of the center of the plume using the possible locations shown in Figure 2. Also present is an uncertainty of ~150 km of influence along the southern portion of the AR (marked in Figure 8).

Our estimates of  $R_{AR}/R_{RR}$  and  $W_{AR}/W_{RR}$  for the Iceland hotspot are 0.54-0.67 and 0.18-0.40, respectively (Figure 7). When considering the model predictions for how  $W_{AR}/W_{RR}$  changes with volume flux,  $Q$ , the estimated  $W_{AR}/W_{RR}$  of the Iceland hotspot suggests a plume flux between  $\sim 100 - 420 \text{ m}^3/\text{s}$  with a thermally controlled lithosphere, and  $\sim 100-200 \text{ m}^3/\text{s}$  with a dehydration-controlled lithosphere. Both flux ranges are consistent with the flux ( $200 \text{ m}^3/\text{s}$ ) simulated by Ito et al. (1999) and the preferred flux ( $193 \text{ m}^3/\text{s}$ ) simulated by Ribe et al. (1995) for a ridge centered Iceland plume, which were both based on explaining the approximate width (1400-1600 km) of the anomalously shallow ridge and thick crust. The current flux estimates are greater than the published estimates ( $30-45 \text{ m}^3/\text{s}$ ) based on the narrower width of the geochemical anomaly of  $\sim 920 \text{ km}$  (Ribe and Delattre, 1998; Schilling, 1991). Our estimates of  $R_{AR}/R_{RR}$  for the North Atlantic fall between model predictions for cases with and without dehydration stiffening (Figures 7). This finding suggests that the rheology of the mantle is intermediate between the temperature- and dehydration- (plus temperature) dependent rheology simulated.

#### 4.2 Crustal thickness

Comparisons of seismically measured crustal thickness near the AR with some example model predictions are shown in Figure 8. The first comparison is along the SE to NW seismic refraction transect from the Norwegian margin to the central portion of the AR from Figure 3 (Breivik et al. 2006, location marked in Figure 1). Again, the models do not predict the large crustal thickness near to the onset of rifting due to initially thick continental lithosphere inhibiting melting as previously noted. From  $\sim 50 \text{ Ma}$  onward, however, the models generally match the overall trend of the observed decreasing crustal thickness with time. Cases with higher versus lower Rayleigh numbers (lower versus higher average viscosity) produce thicker versus thinner crust at a similar plume volume flux. The models of a dehydrated lithosphere produce thinner crust and a more subtle decrease in crustal thickness over time compared to models of a thermal lithosphere. Cases with higher plume volume flux predict a wider plume pancake and thus produce thicker crust than those with lower flux. For both types of rheologies, models of a lower plume flux ( $114-146 \text{ m}^3/\text{s}$ ) predict crustal thicknesses qualitatively similar to those observed. This result supports those based on  $W_{AR}/W_{RR}$  for plume fluxes of  $100-200 \text{ m}^3/\text{s}$  (Figure 7).

Figure 8c-d shows model predictions versus seismically derived crustal thickness (Rai et al., 2012) from south to north along the  $\sim 30 \text{ Myr}$  isochron on the SE side of AR (location marked in Figure 1). The seismic profile shows crustal thickness increasing southward in the southern half of AR, where spreading was slowest, and a more-or-less uniform crustal thickness in the northern half of the AR. The trend of increasing crustal thickness with decreasing spreading rate is opposite the trend of normal oceanic crust, with slower spreading typically resulting in thinner crust (White et al., 2001), and is therefore good evidence that the southern portion of the AR was influenced by the plume. Indeed models without a plume do not predict a steady N-S change in crustal thickness along the AR. Models of a dehydrated lithosphere produce thinner crust and a smaller southward increase in crustal thickness than the models of a thermal lithosphere. For

both rheologies, models of the highest plume flux predict the plume to influence the whole AR and crust that is much thicker than observed. Models of lower plume flux predict the plume to influence only the southern part of the AR and crustal thicknesses similar to those observed. These results further support a plume with relatively low flux (95-128 m<sup>3</sup>/s).

Crustal thickness measurements along the present-day Mid-Atlantic Ridge, starting at the RR in the south, extending north across Iceland and then along the KR, as presented by Hooft et al. (2006), are compared with model predictions in Figure 9. Like the observations, models show peaks in crustal thickness over the center of the plume on Iceland, a sharp decrease ~200 km north and south of the peak, and gradual decreases in crustal thickness further from the plume center. Hooft et al. (2006) noted an asymmetry in the observed crustal thickness, with the crust along the KR, 200-500 km north of the plume center being 1-2 km thinner than that at the same distance range south along the RR. The models of a dehydrated lithosphere predict the same sense of asymmetry, although slighter greater asymmetry than observed: the model crust is thinner by ~2 km along the KR 200-350 km north of the plume center than the same distance south along the RR. The models of a thermal lithosphere do not predict this sense of asymmetry. In terms of maximum crustal thickness, the models of a dehydrated lithosphere predict thinner crust than observed, whereas the models of a thermal lithosphere predict thicker crust than observed.

Thus, model results for the peak crustal thickness on Iceland, the asymmetry in crustal thickness along the present-day Mid-Atlantic Ridge, as well as the degree of radial asymmetry, measured by  $R_{AR}/R_{RR}$ , at 30 Ma all suggest the actual rheology is intermediate between the two rheologies simulated. In other words, a viscous, dehydrated lithosphere is probably present, but is less viscous than we have simulated. An intermediate behavior may arise if the average viscosity of the whole North Atlantic upper mantle, including the dehydrated layer, is even lower than that modeled. Alternatively, it is possible that non-Newtonian rheology leads to lower viscosities in the dehydrated layer, where strain rates are higher, such as above the plume or near the ridge axis (Ito et al., 2010). Another possibility is that the presence of even a small amount of melt in the mantle substantially reduces viscosity to partially negate the effects of dehydration strengthening (Takei and Holtzman, 2009).

## CHAPTER 5. CONCLUSIONS

Numerical models of plume-ridge interaction are used to study the cause of variations in the influence of the Iceland hotspot along the Mid-Atlantic Ridge and determine the origin of the NE-SW asymmetry evident in the residual topography and crustal thickness. Models initially simulate a plume pancake that spans the full width of the Greenland margin at the time of continental breakup. The pancake is then predicted to contract rapidly as the rifting continental lithosphere advects it away from the ridge, providing a simple explanation for the observed rapid narrowing of Iceland plume influence near the continental margins. Once this initial contraction occurs and half-spreading rates have dropped from  $\sim 32$  to  $\sim 10$  mm/yr, the plume pancake is predicted to widen southward along the Reykjanes Ridge (RR), resembling the observed southward-trending rough-smooth boundary east and west of the RR. To the northeast, the models of a lower plume flux predict the plume pancake to extend along only the southern part of the Aegir Ridge (AR). This prediction is consistent with seismic measurements that reveal a southward increase in crustal thickness only along the southern half of the AR. Thus, an asymmetry in modeled plume influence arises quickly after continental breakup, as is observed in the residual topography and seismic observations. The observed southward progression of the rough-smooth boundary on the seafloor between the 25 Ma isochrons after spreading shifts from the AR to KR is not predicted by the models and could signal an increase in the Iceland plume flux since this time.

All models predict the plume pancake to spread less far along the AR than the RR. The ratio of radial extents of plume influence along the AR and RR ( $R_{AR}/R_{RR}$ ) is predicted to be insensitive to changes in plume volume flux and viscosity, and varies primarily with changes in rheology. When the lithosphere is controlled by dehydration, the plume expands 70-80% along the AR as it does along the RR ( $R_{AR}/R_{RR} = 0.7-0.8$ ). This result indicates that the asymmetry is caused partly by the asymmetric configuration of the ridges relative to the plume center (ridge geometry control, hypothesis 1). Specifically, the locations of the AR east of, and the RR directly over the plume center creates a situation in which North American plate motion opposes the expansion of plume material NE toward the AR, with no such opposing motion SSW along the RR. With a thermal lithosphere,  $R_{AR}/R_{RR} = 0.4-0.5$ ; this enhanced asymmetry is due to the topography of the base of a thermal lithosphere (lithosphere thickness variation, hypotheses 2), which creates relatively thick lithosphere between the plume center and the AR that further inhibits NE plume expansion to the AR, but thin lithosphere beneath the RR, which facilitates SSW plume expansion.

Models of Iceland plume volume fluxes of 100-200 m<sup>3</sup>/s best explain observed ratios of the widths of plume influence along the AR and RR ( $W_{RR}/W_{AR}$ ), as well as crustal thickness along the RR and AR at  $\sim 30$  Ma. Comparisons of observed and modeled asymmetry in radial distance of plume influence ( $R_{AR}/R_{RR}$ ) at 30 Ma and crustal thickness along the present-day Mid-Atlantic ridge suggest that there is a dehydrated lithosphere, but one that is less viscous than simulated in models.

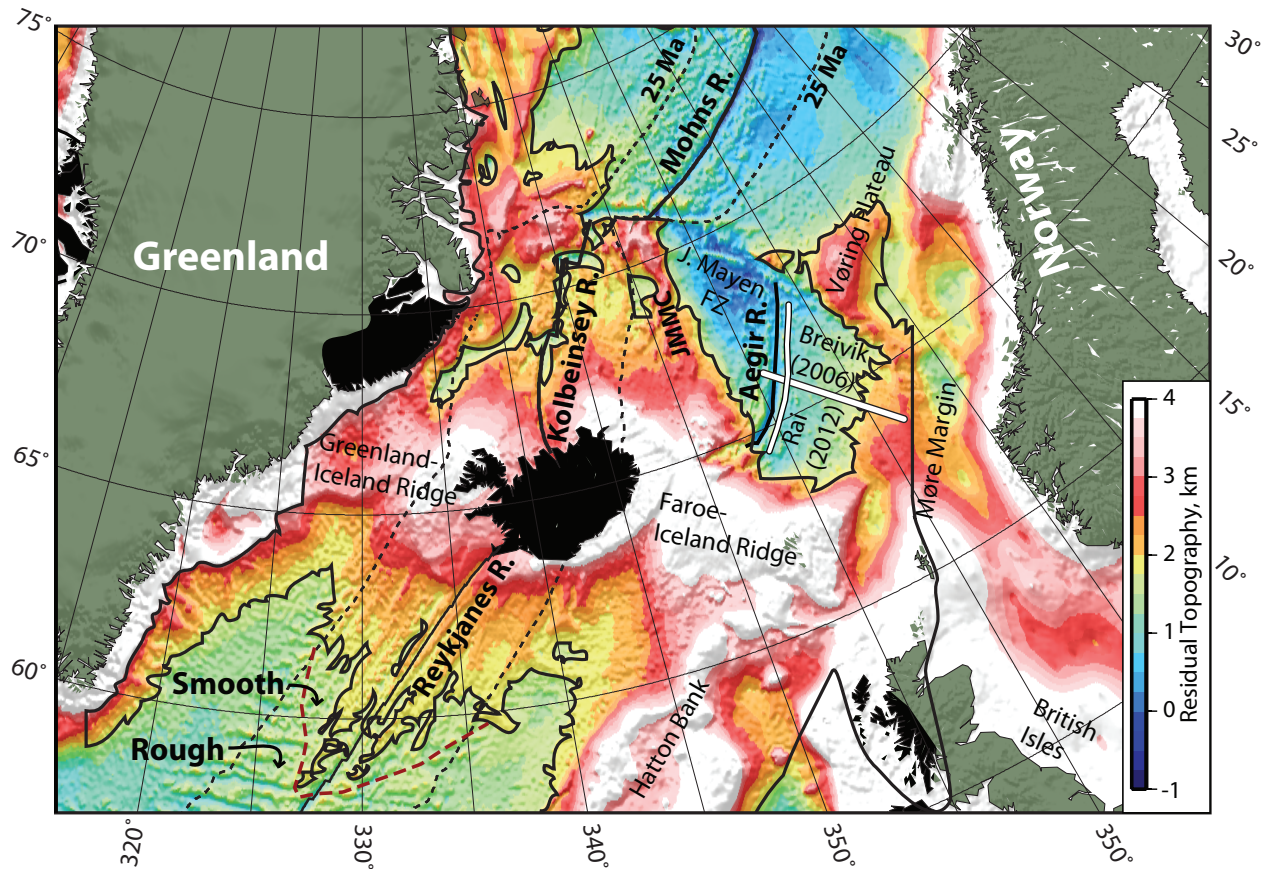


**Figure 1:** Residual basement topography of the North Atlantic (Ito and van Keken, 2007). Narrow dashed lines mark the 25 Ma isochrons (Müller et al., 2008), approximately when the Aegir Ridge ceased spreading. Black outlines enclose areas with  $> 1.8$  km residual topography and the approximate area of hotspot influence (Mjelde et al., 2005; Nielsen and Hopper, 2004). The dashed red line marks the transition between smooth seafloor created by the part of the RR spreading obliquely in the north without any prominent transform faults, in contrast to the rougher seafloor to the south created by orthogonal spreading along segments separated by transform faults (White, 1997). The solid white lines show seismic Profile 1-03 of Breivik et al. (2006) and the seismic line of Rai et al. (2012).

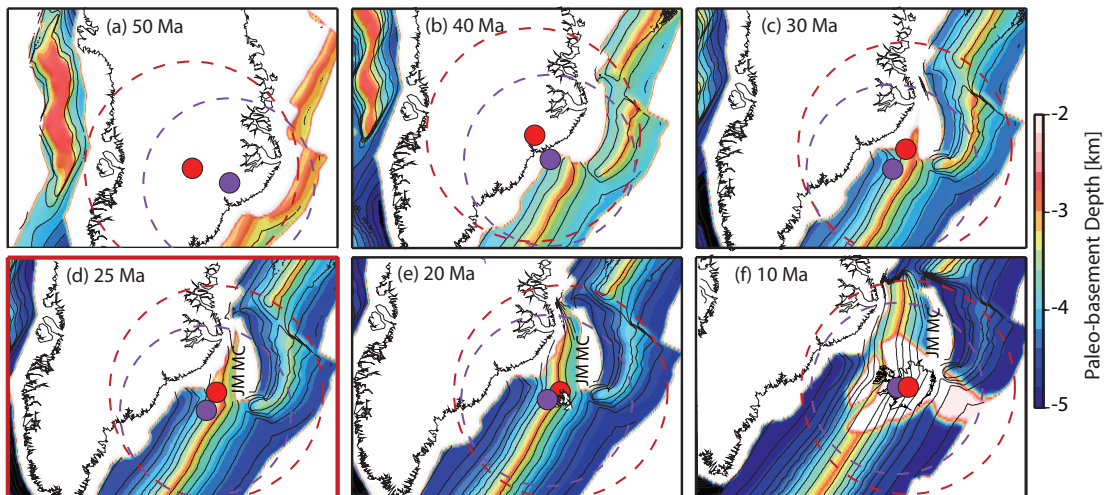


**Figure 2:** Plate reconstructions and paleo-basement depth (Müller et al., 2008). Filled circles mark estimated center of hotspot relative to Greenland by Lawver and Müller (1994) (red) and Mihalfy et al. (2008) (purple). Dashed circles show corresponding (like colors) areas of influence of the Iceland plume for perfectly circular plume pancakes when the Aegir Ridge became extinct ~25 Ma, based on the distance to the rough-smooth boundary in seafloor fabric created at the Reykjanes Ridge at 25 Ma.

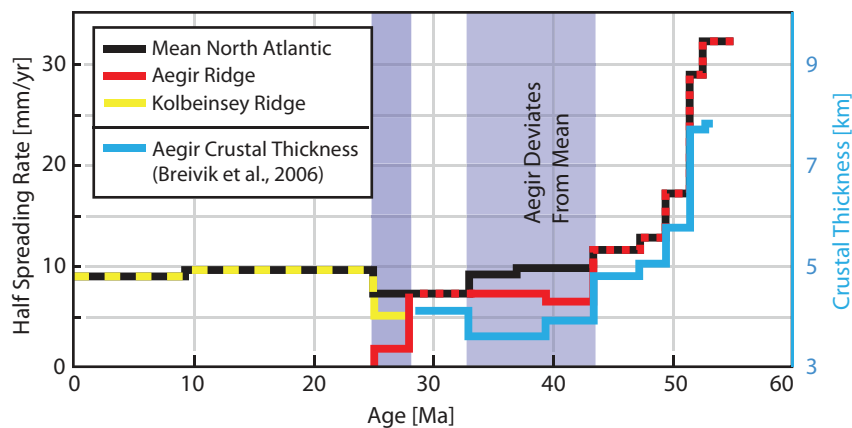


**Figure 3:** Geological estimates of the spreading rates at MR (Breivik et al., 2009; Voss et al., 2009), RR (Smallwood and White, 2002), AR (Breivik et al., 2006), and KR (yellow, Mosar et al., 2002) were averaged to create a mean North Atlantic spreading rate through time (black). Since 33 Ma, spreading rates by Mosar et al. (2002) for all four ridges are incorporated. The mean spreading rate (black) was used to model all of the active ridges at times when the geological estimates of their spreading rates were very similar (deviating by  $< 2$  mm/yr). However, during times marked by shaded bands, the model Aegir and Kolbeinsey Ridges were assigned the low rates defined by the geological estimates, and the model Reykjanes and Mohns Ridges shared the same (faster) spreading rate, determined by the average (black) of their individual geological rates.

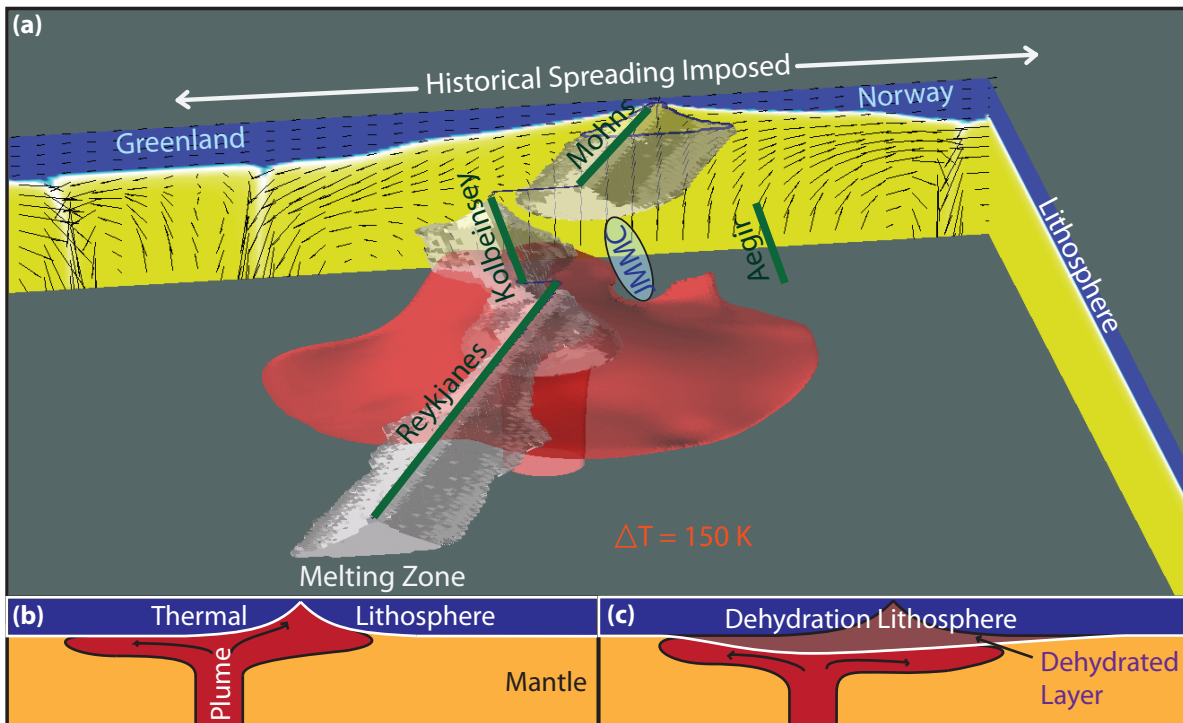


**Figure 4:** Example predictions (a) from Model 3a at a model time corresponding to present-day. Green lines show the imposed ridge geometry, the red isosurface envelopes mantle with temperature  $\geq 55^\circ\text{C}$  above the ambient mantle potential temperature, the gray isosurface surrounds regions of melting, the boundary walls show temperature (colors, lithosphere in light blue, asthenosphere in yellow), with arrows representing material velocities. Some details of the recent ridge and hotspot configuration are neglected; the eastward jumps in the Eastern Rift Zone on Iceland (Hardarson et al., 1997) are replaced by a straight, fixed RR. Also, the plume is centered on the modeled RR, and therefore is offset  $\sim 200$  km WNW from the present-day plume center imaged with mantle tomography (Allen et al., 2002; Wolfe et al., 1997). See text for further justification. Cartoons illustrate the mantle plume (red) rising and expanding beneath a (b) “thermal lithosphere” (blue), the base of which corresponds to the thermal boundary layer and a (c) “dehydrated” lithosphere (blue, purple), the base of which corresponds to the dry-solidus.

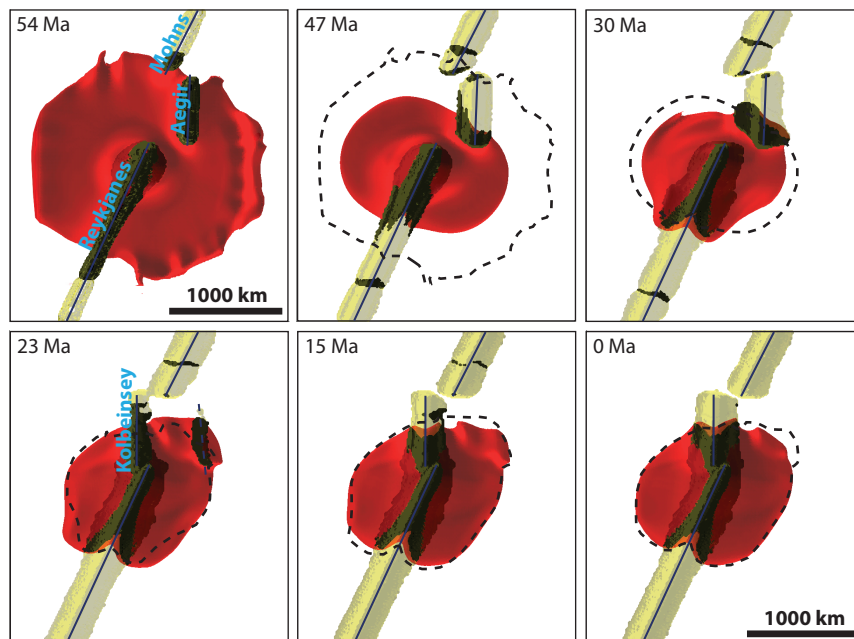


**Figure 5:** Snap shots at different times of Model 3a (Table 1) in which the plume has a relatively high flux ( $Q = 232 \text{ m}^3/\text{s}$ ), low Rayleigh number ( $0.5 \times 10^6$ ), and the lithosphere is thermally controlled (no dehydration rheology). Red isosurface envelops mantle with excess temperature  $\geq 55 \text{ }^\circ\text{C}$ ; yellow isosurface marks melt production; black isosurface marks material melting that originated in the plume stem. Active spreading centers are marked with black lines. To show how the plume pancake changes between panels, the dashed black line outlines the plume pancake from the previous panel.

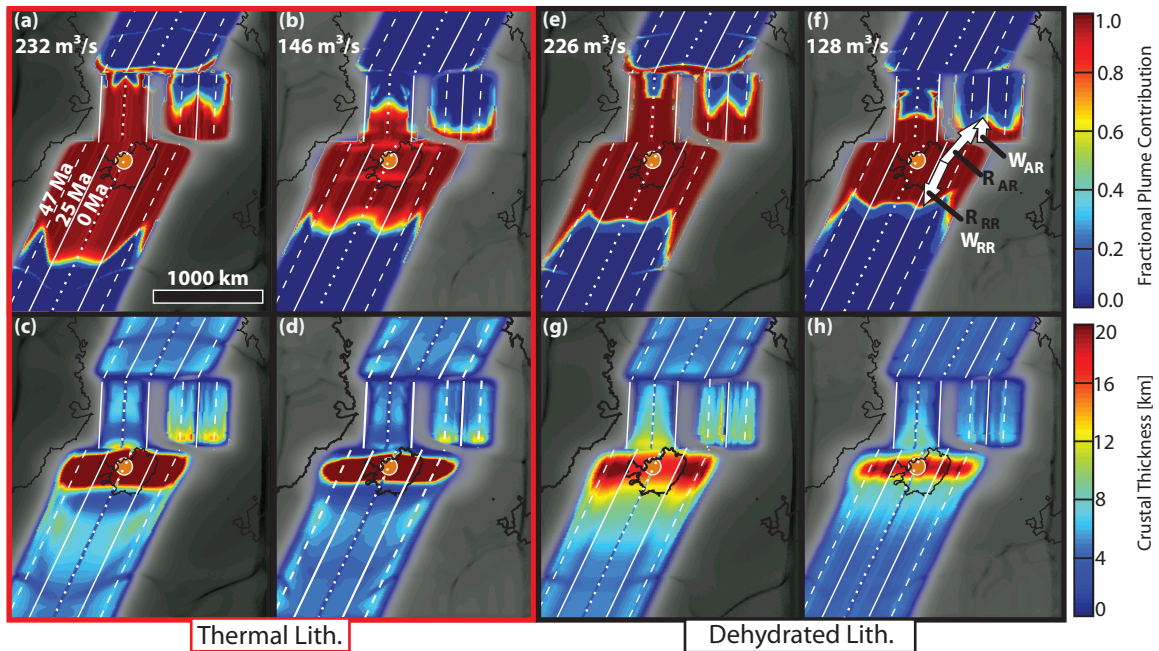


**Figure 6:** (a-d) Maps of two models without dehydration effects on viscosity (i.e., thermal lithosphere, outlined in red). (a,b) Fraction of melt contributed by the plume, and (c,d) model-melt thickness. First column shows Model 3a (same as in Figure 5) of a high plume volume flux,  $Q = 232 \text{ m}^3/\text{s}$ . Second column shows Model 8a of a low plume volume flux,  $Q = 146 \text{ m}^3/\text{s}$ . Color scale for melt thickness is saturated at 20 km; maximum thickness for the two cases are 138 km (column one), and 90 km (column two). (e-h) Maps of two models with dehydration effects on viscosity (i.e., dehydrated lithosphere). Third column shows Model 4, of a higher plume volume flux,  $226 \text{ m}^3/\text{s}$ ; fourth column shows Model 8b, of a lower plume volume flux,  $128 \text{ m}^3/\text{s}$  (right). Color scale for melt thickness is saturated at 20 km; maximum thickness for the two cases are 21 km (column 3), and 17 km (column 4). Arrows on (f) illustrate measurements of widths of plume extent. Measurements were taken at a model output time of 30 Ma, resulting in an AR used in the illustration that has migrated east of the ridge location used in the model analysis.

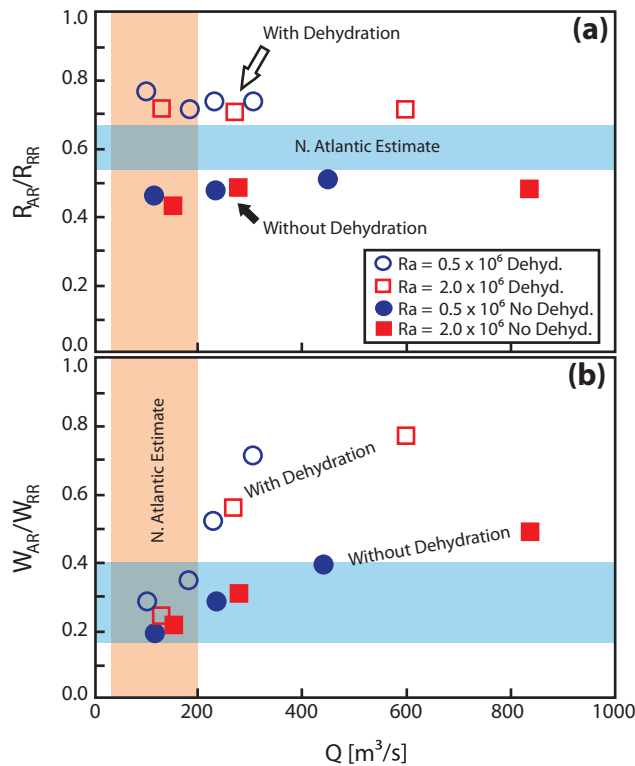


**Figure 7:** Results of models run at two Rayleigh numbers vs. plume flux,  $Q$ . (a) Ratio of radial extent of the plume along the Aegir Ridge,  $R_{AR}$ , relative to that along the Reykjanes Ridge,  $R_{RR}$ , (See Figure 6f) and (b) the ratio of width of plume influence along the Aegir Ridge axis,  $W_{AR}$ , to that along the Reykjanes Ridge axis,  $W_{RR}$  (See Figure 6f). Open and solid shapes represent cases with and without a dehydration rheology, respectively. Shaded blue bands show estimates for the same ratios with uncertainties for the Iceland hot spot as described in the text. Shaded red bands show estimates for Iceland plume flux that span values used over a range of studies (e.g. Ito et al., 1999; Ribe et al., 1995; Ribe and Delattre, 1998).

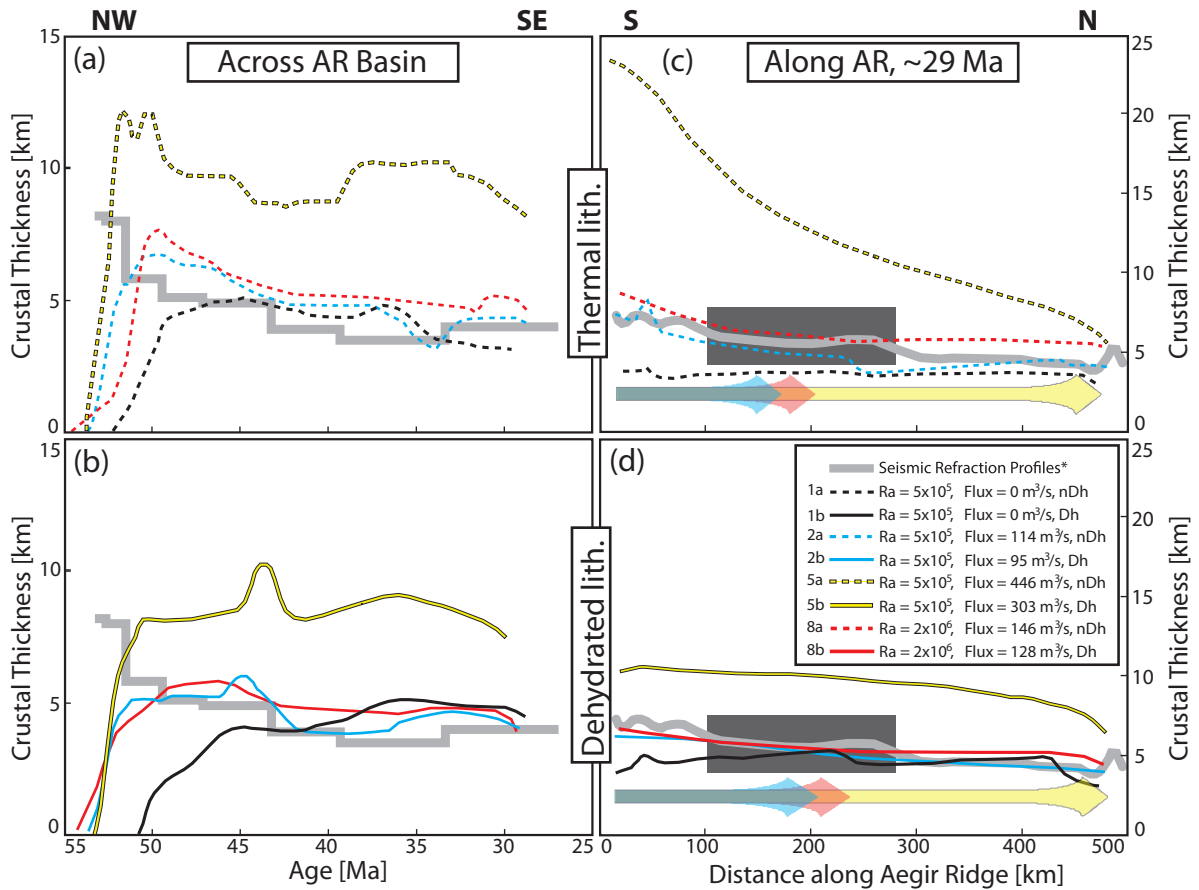


**Figure 8:** (a,b) Profile of crustal thickness vs. age (gray) along a SE-to-NW profile starting at the Møre Margin and extending towards the Aegir Ridge, after Breivik et al. (2006). Colored curves show prediction for models of a (a) thermal lithosphere and (b) dehydrated lithosphere. (c,d) Profile of crustal thickness vs. distance along the Aegir Ridge (gray) along the south-to-north profile of Rai et al. (2012) for cases with a (c) thermal lithosphere and (d) dehydrated lithosphere. In (c,d) large arrows show the predicted extent of model plume influence on the ridges. The gray box shows the range of plausible observed plume influence inferred from the seismically measured crustal thickness variations. Models and their key parameters are labeled in the legend. Black solid and dashed lines are predictions of models without a plume.

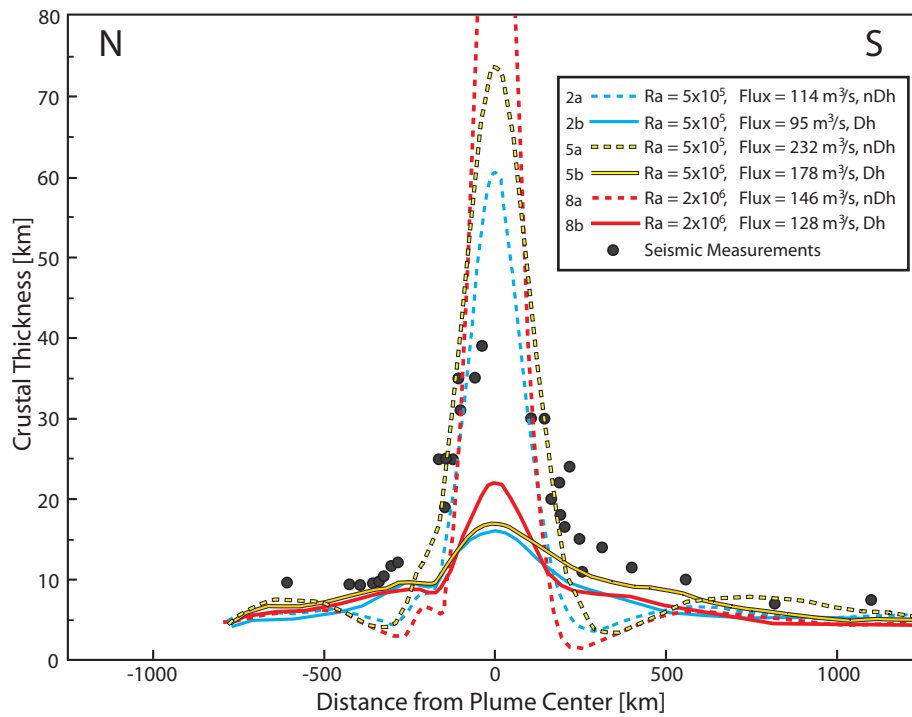


**Figure 9:** Crustal thickness profiles taken along the Reykjanes Ridge, across Iceland, and along the Kolbeinsey Ridge. Filled circles represent seismic measurements presented by Hooft et al., (2006); colored curves show crustal thickness of model predictions versus distance from the center of the plume along the ridges. Curves are for the same models as in Figure 8.

## REFERENCES

- Allen, R.M., Nolet, G., Morgan, W.J., Vogfjord, K., Bergsson, B.H., Erlendsson, P., Foulger, G.R., Jakobsdottir, S., Julian, B.R., Pritchard, M., Ragnarsson, S., Stefansson, R., 2002. Imaging the mantle beneath Iceland using integrated seismological techniques. *J. Geophys. Res.* 107, 10.1029/2001JB000595.
- Ballmer, M., van Hunen, J., Ito, G., Tackley, P.J., Bianco, T.A., 2007. Non-hotspot volcano chains originating from small-scale sublithospheric convection. *Geophys. Res. Lett.* 34, L23310, doi:10.1029/2007GL031636.
- Bianco, T.A., Ito, G., Hunen, J.v., Ballmer, M.D., Mahoney, J.J., 2008. Geochemical variation at the Hawaiian hotspot caused by upper mantle dynamics and melting of a heterogeneous plume. *Geochem. Geophys. Geosyst.* 9, Q11003.
- Breivik, A.J., Faleide, J.I., Mjelde, R., Flueh, E.R., 2009. Magma productivity and early seafloor spreading rate correlation on the northern Vøring Margin, Norway — Constraints on mantle melting. *Tectonophysics* 468, 206-223.
- Breivik, A.J., Mjelde, R., Faleide, J.I., Murai, Y., 2006. Rates of continental breakup magmatism and seafloor spreading in the Norway Basin–Iceland plume interaction. *J. Geophys. Res.* 111, B07102.
- Coffin, M.F., Eldholm, O., 1994. Large igneous provinces: Crustal structure, dimensions, and external consequences. *Rev. Geophys.* 32, 1-36.
- Dick, H.J.B., Lin, J., Schouten, H., 2003. An ultraslow-spreading class of ocean ridge. *Nature* 426, 405-412.
- Hardarson, B.S., Fitton, J.G., Ellam, R.M., Pringle, M.S., 1997. Rift relocation—a geochemical and geochronological investigation of a paleo-rift in northwest Iceland. *Earth Planet. Sci. Lett.* 153, 181-196.
- Hirth, G., Kohlstaedt, D.L., 2003. Rheology of the upper mantle and the mantle wedge: A view from the experimentalists, in: Eiler, J. (Ed.), *Inside the Subduction Factory*, *Geophys. Monogr. Ser. AGU*, Washington D.C., pp. 83-105.
- Holbrook, W.S., Larsen, H.C., Korenaga, J., Dahl-Jensen, T., Reid, I.D., Kelemen, P.B., Hopper, J.R., Kent, G.M., Lizarralde, D., Bernstein, S., Detrick, R.S., 2001. Mantle thermal structure and active upwelling during continental breakup in the North Atlantic. *Earth Planet. Sci. Lett.* 190, 251-266.
- Hooft, E.E., Brandsdottir, B., Mjelde, R., Shimamura, H., Murai, Y., 2006. Asymmetric plume-ridge interaction around Iceland: The Kolbeinsey Ridge Iceland Seismic Experiment. *Geochem. Geophys. Geosyst.* 7, 1-26.
- Ito, G., Dunn, R., Forsyth, D.W., 2010. A study of short-period surface wave data, geodynamic models, and the rheology and dynamics of the mantle beneath the East-Pacific Rise, Fall Meeting, AGU, San Francisco, CA, Abstract DI34A-01.
- Ito, G., Shen, Y., Hirth, G., Wolfe, C., 1999. Mantle flow, melting, and dehydration of the Iceland mantle plume. *Earth Planet. Sci. Lett.* 165, 81-96.
- Ito, G., van Keken, P.E., 2007. Hot spots and melting anomalies, in: Bercovici, D. (Ed.), *Mantle Dynamics*. Elsevier, Amsterdam, The Netherlands, pp. 371-435.
- Katz, R.F., Spiegelman, M., Langmuir, C.H., 2003. A new parameterization of hydrous mantle melting. *Geochem. Geophys. Geosyst.* 4, 173, doi:10.1029/2002GC000433.

- Lawver, L.A., Müller, R.D., 1994. The Iceland hotspot track. *Geology* 22, 311-314.
- Mihalffy, P., Steinberger, B., Schmelting, H., 2008. The effect of the large-scale mantle flow field on the Iceland hotspot track. *Tectonophysics* 447, 5-18.
- Mjelde, R., Breivik, A.J., T.Raum, Mittelstaedt, E., Ito, G., Faleide, J.I., 2008. Magmatic and tectonic evolution of the North Atlantic. *J. Geol. Soc.* 165, 32-42.
- Mjelde, R., Raum, T., Myhren, B., Shimamura, H., Murai, Y., Takanami, T., Karpuz, R., Næss, U., 2005. Continent-ocean transition on the Vøring Plateau, NE Atlantic, derived from densely sampled ocean bottom seismometer data. *J. Geophys. Res.* 110, doi:10.1029/2004JB003026.
- Moresi, L., Gurnis, M., 1996. Constraints on the lateral strength of slabs from three-dimensional dynamic flow models. *Earth Planet. Sci. Lett.* 138, 15-28.
- Mosar, J., Lewis, G., Torsvik, T.H., 2002. North Atlantic sea-floor spreading rates: implications for the Tertiary development of inversion structures of the Norwegian–Greenland Sea. *J. Geol. Soc. London* 158, 503–515.
- Müller, R.D., Sdrolias, M., Gaina, C., Roest, W.R., 2008. Age, spreading rates, and spreading symmetry of the world's ocean crust. *Geochem. Geophys. Geosyst.* 9, Q04006.
- Nielsen, T.K., Hopper, J.R., 2004. From rift to drift: Mantle melting during continental breakup. *Geochem. Geophys. Geosyst.* 5, 7, doi:10.1029/2003GC000662.
- Rai, A.K., Breivik, A.J., Mjelde, R., Hanan, B.B., Ito, G., Sayit, K., Howell, S., Vogt, P.R., Pedersen, R.-B., 2012. Analysis of converted S-waves and gravity anomaly along the Aegir Ridge: implications for crustal lithology, Fall Meeting, AGU, San Francisco, Abstract T31B-2587.
- Ribe, N., Christensen, U.R., Theissing, J., 1995. The dynamics of plume-ridge interaction, 1: Ridge-centered plumes. *Earth Planet. Sci. Lett.* 134, 155-168.
- Ribe, N., Delattre, W.L., 1998. The dynamics of plume-ridge interaction, 3: The effects of ridge migration. *Geophys. J. Int.* 133, 511-518.
- Schilling, J.-G., 1999. Dispersion of the Jan Mayen and Iceland mantle plumes in the Arctic: A He-Pb-Nd-Sr isotope tracer study of basalts from the Kolbeinsey, Mohns, and Knipovich Ridges. *J. Geophys. Res.* 104, 10,543–510,569.
- Schilling, J.-G., Zajac, M., Evans, R., Johnston, T., White, W., Devine, J.D., Kingsley, R., 1983. Petrologic and geochemical variations along the Mid-Atlantic Ridge from 29°N to 73°N. *Amer. J. Sci.* 283, 510-586.
- Schilling, J.G., 1991. Fluxes and excess temperatures of mantle plumes inferred from their interaction with migrating mid-ocean ridges. *Nature* 352, 397-403.
- Smallwood, J.R., Staples, R.K., Richardson, K.R., White, R.S., 1999. Crust generated above the Iceland mantle plume: From continental rift to oceanic spreading center. *J. Geophys. Res.* 104, 22,885-822,902.
- Smallwood, J.R., White, R.S., 2002. Ridge-plume interaction in the North Atlantic and its influence on continental breakup and seafloor spreading. Geological Society, London, Special Publications 197, 15-37.
- Steinberger, B., 2000. Plumes in a convecting mantle: Models and observations for individual hotspots. *J. Geophys. Res.* 105, 11,127-111,152.
- Takei, Y., Holtzman, B.K., 2009. Viscous constitutive relations of solid-liquid composites in terms of grain boundary contiguity: 1. Grain boundary diffusion control model. *J. Geophys. Res.* 114.

- Vink, G.E., 1984. A hotspot model for Iceland and the Voring Plateau. *J. Geophys. Res.* 89, 9949-9959.
- Vogt, P.R., Johnson, G.L., 1975. Transform Faults and Longitudinal Flow Below the Midoceanic Ridge. *J. Geophys. Res.* 80, 1399-1428.
- Voss, M., Schmidt-Aursch, M.C., Jokat, W., 2009. Variations in magmatic processes along the East Greenland volcanic margin. *Geophys. J. Int.* 177, 755–782.
- White, R.S., 1988. A hot-spot model for early Tertiary volcanism in the N Atlantic. *Geol. Soc. Spec. Publ.* 39, 3-13.
- White, R.S., 1997. Rift-plume interaction in the North Atlantic. *Phil. Trans. R. Soc. Lond. A* 355, 319-339.
- White, R.S., Minshull, T.A., Bickle, M.J., Robinson, C.J., 2001. Melt Generation at Very Slow-Spreading Oceanic Ridges: Constraints from Geochemical and Geophysical Data. *J. Petrol.* 42, 1171-1196.
- Wilson, J.T., 1973. Mantle plumes and plate motions. *Tectonophysics* 19, 149–164.
- Wolfe, C., Bjarnason, I.T., VanDecar, J.C., Solomon, S.C., 1997. Seismic structure of the Iceland mantle plume. *Nature* 385, 245-247.
- Zhong, S., Zuber, M.T., Moresi, L.N., Gurnis, M., 2000. The role of temperature dependent viscosity and surface plates in spherical shell models of mantle convection. *J. Geophys. Res.* 105, 11,063-011,082.